The Chandrayaan-1 X-ray Spectrometer: First Results

S.Z. Weider[1,2,3,4*], B.J. Kellett[3], B.M. Swinyard[3,5], I.A. Crawford[1,2], K.H. Joy[1,2,6], M. Grande[7], C.J. Howe[3], P. Sreekumar[8], J. Huovelin[9], S. Narendranath[8], L. Alha[9], M. Anand[10,11], P.S. Athiray[8], N. Bhandari[12], J. Carter[7], A.C. Cook[7], L.C. d'Uston[13,14], V.A. Fernandes[15], O. Gasnault[13,14], J.N. Goswami[12], J.P.D. Gow[16], A.D. Holland[16], D. Koschny[17], D.J. Lawrence[18], B.J. Maddison[3], S. Maurice[13,14], D.J. McKay[3], T. Okada[19], C. Pieters[20], D. Rothery[11], S.S. Russell[10], A. Shrivastava[8], D.R. Smith[21] and M. Wieczorek[22].

[1] Department of Earth and Planetary Sciences, Birkbeck College, Malet Street, London WC1E 7HX, UK.

[2] Centre for Planetary Science at UCL/Birkbeck, Department of Earth Sciences, Gower Street, London, WC1E 6BT, UK.

[3] RAL Space, Rutherford Appleton Laboratory, Didcot, Oxon, OX11 0QX, UK.

[4] Department of Terrestrial Magnetism, Carnegie Institution of Washington, Washington DC, 20015, USA.

[5] Department of Physics and Astronomy, UCL, Gower Street, London, WC1E 6BT, UK.

[6] Center for Lunar Science and Exploration, The Lunar and Planetary Institute, USRA, 3600 Bay Area Blvd., Houston, Texas 77058, USA.

[7] Institute of Mathematical and Physical Sciences, University of Wales, Aberystwyth, Ceredigion, SY23 3BZ, UK.

[8] Indian Space Research Organisation, Bangalore, India.

[9] Division of Geophysics and Astronomy, Department of Physics, PO Box 48, FI-00014, University of Helsinki, Finland.

[10] Department of Mineralogy, Natural History Museum, Cromwell Road, London, SW7 5BD, UK.

[11] Department of Earth and Environmental Sciences, Open University, Milton Keynes, MK7 6AA, UK.

[12] Physical Research Laboratory, Navrangpura, Ahmedabad, 380009, India.

[13] Université de Toulouse, UPS-OMP, IRAP, Toulouse, France.

[14] CNRS, IRAP, 9 av. Colonel Roche, BP 44346, F-31028 Toulouse cedex 4, France.

[15] Institute of Physics, University of Bern, Sidlerstrasse 5, CH-3012, Berne, Switzerland.
[16] e2v centre for electronic imaging, PSSRI, The Open University, Milton Keynes, MK7 6AA, UK.
[17] European Space Agency, ESTEC, The Netherlands.
[18] Applied Physics Laboratory, Johns Hopkins University, USA.
[19] Institute of Space and Astronautical Science, Japan Aerospace Exploration Agency, Sagamihara, Kanagawa, 229-8510, Japan.
[20] Brown University, RI, USA.
[21] Centre for Sensors and Instrumentation, School of Engineering and Design, Brunel University, Uxbridge, Middlesex, UB8 3PH, UK.
[22] Institut de Physique du Globe de Paris, Univ Paris Diderot, 4 Avenue de Neptune, F-94100 Saint Maur des Fossés, France.

*Corresponding author. Email: sweider@ciw.edu.

Keywords: Lunar X-ray spectroscopy; Lunar regolith; Lunar chemistry; Lunar crust; Gamma-ray spectroscopy

Abstract

We present X-ray fluorescence observations of the lunar surface, made by the Chandrayaan-1 X-ray Spectrometer during two solar flare events early in the mission (12th December 2008 and 10th January 2009). Modelling of the X-ray spectra with an abundance algorithm allows quantitative estimates of the MgO/SiO_2 and Al_2O_3/SiO_2 ratios to be made for the two regions, which are in mainly basaltic areas of the lunar nearside. One of these ground tracks includes the Apollo 14 landing site on the Fra Mauro Formation. Within the 1 σ errors provided, the results are inside the range of basaltic samples from the Apollo and Luna collections. The Apollo 14 soil composition is in agreement with the results from the January flare at the 1 σ uncertainty level. Discrepancies are observed between our results and compositions derived for the same areas by the Lunar Prospector gamma-ray spectrometer; some possible reasons for this are discussed.

1. Introduction

Remote sensing of the Moon reveals on a global scale the compositional (Lucey et al., 1998; 2000; Lawrence et al., 2002; 2003; Lucey and Cahill, 2006; Prettyman et al., 2006; Wöhler et al., 2011) and mineralogical (Belton et al., 1994; Pieters and Tompkins, 1999; Lucey, 2004; Pieters et al., 2006; Glotch et al., 2010; Greenhagen et al., 2010) heterogeneities of its surface. Such missions have revealed that the Moon's surface is more diverse than originally thought, based on the studies of the geological samples returned by the Apollo and Luna missions (Taylor et al., 1991; Lucey et al., 2006; Shearer et al., 2006). These remotely sensed data led to the recognition that the Moon can be broadly divided into three compositional terranes (Jolliff et al., 2000) that reflect the surface expression of the Moon's (i) primary crust (the Feldspathic Highlands Terrane), (ii) secondary crust (magmatic and volcanic deposits associated with the nearside Procellarum KREEP Terrane), and (iii) possible lower crust exposed in the South Pole-Aitken Terrane.

The new perspectives provided by compositional remote sensing datasets are fundamental to the understanding of the Moon's geological diversity and history. However, the picture is not yet complete. In particular, some key rock-forming elements, such as Mg, Al, Si and Ca, have only been mapped globally at low spatial resolutions (~150 km per pixel) using gamma-ray spectroscopy (Prettyman et al., 2006), although a recently published method based on optical spectral data (Wöhler et al., 2011) proposes that mapping some of these elements may be possible with higher spatial resolution. X-ray fluorescence (XRF) instruments on Apollo 15 and Apollo 16 (Adler et al., 1972a; 1972b; Adler and Trombka, 1977; Andre et al., 1977) were able to map the distribution of Mg, Al and Si for features down to ~15 km, but for only about a tenth of the lunar surface (Andre et al., 1977), as depicted in Figure 1a. Furthermore, for other key elements (i.e., Ti and Fe) there are significant discrepancies between the Clementine and Lunar Prospector datasets (Lawrence et al., 2002; Gillis et al., 2004; Lucey et al., 2006; Prettyman et al., 2006). Additional XRF detections of Ti and Fe in the lunar surface were made using D-CIXS (Demonstration of a Compact Imaging X-ray Spectrometer) onboard ESA's SMART-1 (Grande et al., 2007; Swinyard et al., 2009), but these have very limited extent and spatial resolution. As such, the tasks of characterising the compositional heterogeneity of the lunar

surface, identifying surface expressions of key lithologies, and interpreting this information in terms of the Moon's evolution remain unfinished. Figure 1a summarises the extent of the lunar surface that has been mapped compositionally with XRF by the Apollo 15 and 16, D-CIXS and C1XS (Chandrayaan-1 X-ray Spectrometer) instruments. The new C1XS dataset (uncalibrated data is currently available to the public in the PDS; a calibrated dataset should be released later in 2011) covers approximately 5% of the lunar surface that has not been previously mapped by XRF. The majority of these data pertain to Mg, Al and Si, but in select cases (e.g., data presented by Narendranath et al., 2011) other elements (i.e., Ca and Fe) were also detected.

2. The C1XS instrument and X-ray fluorescence

C1XS was a compact X-ray spectrometer (Grande et al., 2009a; 2009b; Howe et al., 2009) that flew onboard Chandrayaan-1, India's first mission to the Moon (Bhandari, 2005; Goswami and Annadurai, 2009). The mission operated in a lunar mapping orbit from December 2008 until its premature end in August 2009. The experiment utilised planetary X-ray fluorescence spectroscopy to measure the abundances of major rock forming elements in the lunar surface. The technique is only possible for atmosphere-free bodies in the inner solar system, where the flux of incident solar X-rays is high enough to cause fluorescent X-ray emission from the uppermost hundred microns in the planetary surface (Yin et al., 1993). The emitted X-rays are characteristic of elements from which they originate and they can therefore be used to help constrain variations in local surface geology. Normal levels of solar intensity result in the excitation of low atomic number elements, including several common in rock-forming minerals such as Mg, Al and Si. During solar flares, intense levels of solar X-rays are emitted and the excitation of heavier atomic-number elements such as K, Ca, Ti and Fe can also occur. A detailed description of the scientific goals of the instrument has been given by Crawford et al. (2009) and a full explanation of the technique is given by Clark and Trombka (1997).

C1XS exploited technology inherited from the D-CIXS instrument on ESA's SMART-1 mission (Grande et al., 2003; 2007; Swinyard et al., 2009). The instrument consisted of 24 nadir pointing swept charge device (SCD) detectors (Holland et al., 2004; Smith et al., 2007; Smith and Gow, 2009) that provided high detection efficiency in the 1 – 7 keV energy range containing the X-ray

fluorescence lines of elements of interest. Micro-machined gold-coated collimators provided a 28° (full width) field of view (FOV), equivalent to a 50 km (1.65˚ arc length) surface footprint from Chandrayaan-1's initial 100 km altitude orbit, and 100 km from its later (i.e., after 19th May 2009) raised orbit of 200 km. A controllable, 5 mm-thick aluminium door provided radiation shielding for the instrument during the launch and cruise phases, and contained a ^{55}Fe calibration source for each SCD detector. Full details of the instrument design and onboard data processing methodology can be found in Howe et al. (2009). The instrument's detection efficiency was derived as 42% at 1.48 keV from pre-flight laboratory measurements (Narendranath et al., 2010a) and in-flight calibrations provided the FWHM of the SCDs: 163 eV at 5.9 keV and -8ºC (Narendranath et al. 2011).

The XRF flux from a planetary surface is highly dependent on the intensity and shape of the incident solar X-ray spectrum, which is highly variable even on short timescales (e.g., Donnelly, 1976; Bouwer, 1983; Crosby et al., 1993). To make quantitative estimates of elemental abundances in planetary regoliths via XRF spectroscopy it is therefore necessary to obtain an accurate measure of the solar X-ray spectrum and the planetary XRF spectrum simultaneously. For this reason C1XS was accompanied on Chandrayaan-1 by an X-ray Solar Monitor (XSM) instrument (Alha et al., 2009), which was based on a similar design flown on the SMART-1 mission (Huovelin et al., 2002; Alha et al., 2008). The XSM device consisted of a separate detector unit on the spacecraft that monitored solar X-ray emission. This non-imaging high purity silicon PIN sensor had a collimated wide FOV of 52° radius (circular field), which enabled Sun visibility during a significant fraction of the mission lifetime. XSM had an energy range (1 – 20 keV), spectral resolution (~250 eV at 5.9 keV) and sensitivity (~8000 counts/s for an X1 flare; 10^{-4} Wm^{-2} in the wavelength range 0.1 – 0.8 nm) and was designed to provide sufficient information on the solar X-ray flux reaching the lunar surface to enable accurate interpretation of the fluorescent lines measured by C1XS. The sensitivity estimate is based on a simulated observation of an X1 flare using an observed solar X-ray spectrum from the SMART-1 XSM, which is rescaled from M-class to X-class and convolved with the response function derived from the calibrations of the Chandrayaan-1 XSM. However, as discussed in Section 4 below, the data reported here were obtained for A-class flares, an order of magnitude weaker than those XSM was designed to characterise (i.e., B-class flares and above; Alha et al., 2008).

As a consequence, the fluxes from these flares were insufficient for XSM to determine reliably the input spectrum, and other methods therefore had to be adopted to estimate the intensity and shape of the exciting solar spectra.

3. First observations

Shortly after commissioning, C1XS observed XRF from the lunar surface during two A-class solar flares (10^{-8} – 10^{-7} Wm^{-2}) on 12th December 2008 and 10th January 2009. The first of these flares has a ground track (~1150 km in length) that crosses the full latitudinal extent of Mare Serenitatis, and also samples the highland areas to the north and south (see Table 1 and Figure 1b). It passes through lava flows within Mare Serenitatis that likely erupted between ~3.8 Ga and ~2.8 Ga (according to the crater-count ages of Hiesinger et al., 2000). These lava flows appear (see Figure 2) to be low-Ti basalts (~3 – 4 wt. % TiO_2) with relatively high FeO contents (~16 – 20 wt. %). The feldspathic highland regions at the north and south of the ground track are characterised by lower FeO and TiO_2 concentrations.

The second flare observation, on 10th January 2009, follows a track through Mare Insularum, Mare Cognitum and Mare Nubium (see Table 1 and Figure 1b) which includes the Apollo 14 landing site (3º38’43” S; 17º28’17” W) located in the Fra Mauro Formation. The analysis of this flare therefore provides an opportunity to test the C1XS data reduction methodologies (Swinyard et al., 2009; 2010; Narendranath et al., 2010b; Weider et al., 2011) with ground truth information from the Apollo 14 sample collection. The Fra Mauro Formation is interpreted as continuous ejecta from the Imbrium basin (Wilhelms et al., 1987; Stöffler et al., 2006), although it is likely to be intermixed with more locally derived material during ballistic sedimentation (e.g., Morrison and Oberbeck, 1975; Haskin et al., 2002). As such, the Apollo 14 landing site cannot be considered to be representative of either maria or the ancient feldspathic highlands (Lucey et al., 2006). The samples collected tend to be impact breccias with generally basaltic or KREEP-rich compositions (Hiesinger and Head, 2006) and radiometric ages that range from ~3.95 Ga (Stadermann et al., 1991) to ~3.77 Ga (Stöffler et al., 1989; Stadermann et al., 1991). According to Hiesinger et al. (2003), the lava flows that comprise the remaining footprint of this flare range from ~3.1 Ga to ~3.7 Ga. They also tend to have greater TiO_2 concentrations (from ~2.5 up to

187 ~8 wt. %) than those in the 12th December 2008 flare ground track, but with a similar FeO
188 content (see Figure 3).
189
190 **4. Data processing, abundance modelling and sources of error**
191
192 During both the observations described in this paper, C1XS collected X-ray flux data in the time-
193 tagged single pixel mode (see Howe et al., 2009) and were converted into 16 second binned
194 spectra. Pre-flight and in-flight calibration information (Narendranath et al., 2010a), along with
195 instrument housekeeping data were used to calibrate each spectrum. For these observations, data
196 from all 24 detectors were co-added in time in order to obtain sufficient counting statistics.
197 Lunar XRF spectrograms for both flares are shown in Figure 4. In each case an average detector
198 background level was subtracted; these backgrounds were determined from long-integrations
199 obtained during periods of quiet (i.e., undetectable) solar activity. We note that both
200 observations reported here were obtained while the Moon was in the Earth's magnetotail,
201 resulting is somewhat higher background levels than when the Moon is outside the magnetotail.
202 The final background-subtracted, energy-calibrated spectra were then modelled in an abundance
203 algorithm to obtain quantitative elemental abundance estimates for the parts of lunar surface
204 observed.
205
206 The abundance algorithm employed (Swinyard et al., 2009; 2010) has been shown to
207 successfully recover major element abundances within ±1 element wt. % for geological
208 specimens of known composition (Weider et al., 2011). It follows the methods of Clark and
209 Trombka (1997) which modifies the fundamental parameters approach (e.g., He and Van Espen,
210 1991) for the analysis of unknown materials using a wide, polychromatic source of X-rays that is
211 relevant for planetary XRF spectroscopy. In addition to the energy-calibrated, background-
212 subtracted C1XS spectra, the algorithm requires as inputs: (i) a modelled solar spectrum
213 containing both the bremsstrahlung continuum and solar emission lines, (ii) the efficiency of the
214 C1XS instrument as a function of energy, (iii) an arbitrary initial rock composition, and (iv) the
215 phase angle of the observation. Using this information the algorithm iterates around the initial
216 rock composition until a best fit to the C1XS spectrum is found (determined by chi-squared
217 minimisation). Each elemental fluorescence line is tested in isolation, starting with the highest

218 energy lines whose abundances are updated before the next line is modelled. When all the lines
219 have been tested the new values are used as the fixed initial composition and the procedure is
220 repeated until there is no variation between runs (normally two complete iterations).
221
222 The model assumes a fixed Si abundance, thus all the other modelled elemental abundances are
223 relative to the Si abundance chosen. This normalisation is possible because the Si concentration
224 within the lunar regolith only varies between about 18 – 23 elemental wt. % (e.g., Rhodes and
225 Blanchard, 1981; Fruland, 1983, Morris et al., 1983; Simon et al., 1985; McKay et al., 1986;
226 1989; Jerde et al., 1987; 1990). This variation in Si abundance has only a minor effect on the Mg
227 and Al results; much larger uncertainties are introduced to the methodology due to our lack of
228 direct and high spectral resolution knowledge of the incident solar flare spectrum, which
229 dominates over all other uncertainties in the methodology.
230
231 By always expressing results as ratios of two elements inaccuracies due to calibration
232 uncertainties, and variations in XRF intensity caused by physical and compositional differences
233 in the regolith, should mostly be negated (Clark and Trombka, 1997), at least for the three low-
234 energy elements (Mg, Al and Si) considered in this paper (Weider et al., 2011). This issue has
235 been the focus of recent analogue laboratory experiments (e.g., Maruyama et al., 2008; Näränen
236 et al., 2008; Weider et al., 2011) that have investigated the role of viewing geometry and surface
237 roughness on the XRF intensity measured from regolith-like samples. These experiments have
238 demonstrated a phase angle-related increase in XRF from compositionally heterogeneous
239 samples, which is energy dependent, and it may therefore be problematic to express abundances
240 as ratios of two elements that differ significantly in energy (e.g., Si and Fe) for data obtained at
241 phase angles above ~60° (Weider et al., 2011). The same studies (Maruyama et al., 2008;
242 Näränen et al., 2008; Weider et al., 2011) also document a decrease in XRF with increasing
243 grain-size from heterogeneous samples, but such an effect is unlikely to have an impact on the
244 analysis of XRF data from well-mixed (gardened) planetary regoliths such as the Moon's,
245 especially on the large spatial scales involved.
246
247 Although the XSM (see Section 2.1) was flown onboard Chandrayaan-1 in order to measure the
248 solar X-ray spectrum during periods of C1XS data acquisition, the solar X-ray flux during the A-

class flare observations discussed in this paper was insufficient for XSM to reliably characterise the incident spectrum. For this reason an alternative source for an incident solar spectrum is required. We have used the *atomdb* (version 2.0.0) database and modelling software (Harvard Chandra X-ray Center: http://cxc.harvard.edu/atomdb/features_idl_html) for this purpose. This software generates a high-resolution modelled solar spectrum with both the bremsstrahlung continuum and superimposed emission lines at a number of different temperatures. Based on the work of Kay et al. (2003) we estimate that the temperatures of the A-class flares observed here were between about 2.5 MK and 3.1 MK. The flare temperatures cannot have been significantly higher without exciting the Ca K_α line at 3.7 keV which is not observed (see Figure 4). To allow for errors introduced by the uncertainty in the flare temperatures, we have modelled the C1XS spectra using both the upper and lower temperature limits and factored this into our quoted errors on the derived abundances (Section 5).

As described by Swinyard et al. (2010), the C1XS instrument efficiency has been derived from a model based on the expected X-ray absorption properties of the SCD detectors, calibrated with laboratory efficiency measurements of monochromated X-rays conducted during the pre-flight calibration campaign (see also Narendranath et al., 2010a). These measurements were made with the same thresholds and event selection criteria as employed in lunar orbit. The resulting efficiencies were found to be consistent with the SCD efficiency measurements obtained from observations of the Crab Nebula by the D-CIXS instrument on SMART-1 (Grande et al., 2007; Swinyard et al., 2009). We note that our abundance modelling procedure, which ratios abundances relative to Si, is relatively insensitive to the absolute instrument efficiency values, especially for the closely spaced low-energy lines discussed here.

As the initial rock composition for the modelling we adopt the average lunar surface composition derived from Lunar Prospector gamma-ray data (Prettyman et al., 2006; i.e., Mg: 4.35 wt. %; Al: 12.35 wt. %; Ca: 11.29 wt. %; Ti: 0.56 wt. %; Fe: 5.93 wt. %; as noted above Si was fixed at 21.00 wt. %). However, it is important to realise that owing to the iterative nature of the method, the final results obtained for Mg and Al are independent of the assumed initial composition (Weider, 2011). The mean phase angle of each observation, also required by the model, is obtained from the instrument pointing (SPICE) data.

5. Results

5.1. 12th December 2008 flare

The fitted spectrum (between 0.7 keV and 2.5 keV) for the 12th December 2008 flare is shown in Figure 5a, and for a subsection of this flare (whose footprint is entirely within Mare Serenitatis) in Figure 5b. These spectra show the three easily resolved low-energy peaks of Mg K_α (1.25 keV), Al K_α, (1.49 keV) and Si K_α (1.74 keV). Although not resolved in these spectra, we note that the modelling also includes the adjacent K_β lines. These spectra also appear to exhibit weak emission at ~1.00 keV, which may possibly be due to the Na K_α line at 1.04 keV. However, as discussed below, this region in C1XS spectra is likely to be dominated by scattered solar X-rays making any such assignment uncertain. The modelled abundances for Mg and Al are given in Table 2. The mean MgO/SiO_2 and Al_2O_3/SiO_2 ratios (averaged from the modelling at the two flare temperatures) for both flare sections are given in Table 3, along with errors which combine the 1 σ fitting errors and the range that arises from the modelling at two flare temperatures. These values are also shown in Figure 6a, where the C1XS results are compared to various lunar samples and Lunar Prospector values.

5.2. 10th January 2009 flare

Figure 5c shows the fitted spectrum for the whole of the 10th January 2009 flare. Figure 5d shows the spectrum for a subsection corresponding to the Fra Mauro Formation which includes the Apollo 14 landing site. The modelled elemental abundances for these spectra are given in Table 2 and the resulting MgO/SiO_2 and Al_2O_3/SiO_2 ratios are given in Table 3. These are compared to lunar samples and Lunar Prospector values in Figure 6b.

Again, these spectra possibly exhibit a weak emission at ~1.00 keV, which could be due to the Na K_α line. Moreover, this emission appears stronger in the Fra Mauro section of the ground track (Figure 5d). The observed line strength would imply a Na abundance of between ~1.10 ± 0.28 wt. % and 1.65 ± 0.48 wt. % (~1.5 to 2.2 wt. % Na_2O), depending on the flare

311 temperature. This would be consistent with the average Apollo 14 soil composition being
312 considerably richer in Na_2O (0.70 wt. %) than for all the other landing sites, whose values are
313 between 0.31 wt. % and 0.54 wt. % (McKay et al., 1991). If this interpretation is correct, then
314 these observations would represent the first XRF observation of Na on the Moon. However, as
315 noted above, the spectral region of the Na K_α line is expected to be dominated by scattered solar
316 lines which, depending on the scattering efficiency, could mimic the emission of lunar Na XRF.
317 We illustrate this in Figure 7, which clearly shows that for high scattering efficiency the entire
318 Na 'line' could be due to scattered solar lines, whereas the neighbouring Mg, Al and Si lines are
319 essentially unaffected. We therefore have to caution that any interpretation of this feature as
320 being due to Na XRF alone can only be tentative as it is not possible with these data to
321 unambiguously fit the level of the scattered solar spectrum.
322
323 **6. Discussion**
324
325 6.1. 12th December 2008 flare
326
327 The C1XS element ratios (with 1 σ errors) for the mare basalt region of Mare Serenitatis
328 (Figure 2) are within the compositional range of mare basalts (Figure 6a). Data collected from
329 the whole flare footprint (Figure 2) have higher Al_2O_3/SiO_2 ratios, consistent with its ground
330 track including feldspathic highland areas at its two ends. Generally, the Lunar Prospector
331 gamma-ray compositions for the flare region overlap with the C1XS results in terms of
332 Al_2O_3/SiO_2 within the 1 σ errors, but the C1XS results are consistently lower in terms of
333 MgO/SiO_2. There could be three possible reasons (or a combination of these) for this
334 discrepancy: (i) the C1XS results presented here are inaccurate; (ii) the Lunar Prospector results
335 presented by Prettyman et al. (2006) are inaccurate; or (iii) there is an intrinsic problem with
336 comparing planetary XRF and gamma-ray spectroscopy data. The likelihood of these options is
337 discussed further in Section 6.4.
338
339 6.2. 10th January 2009 flare
340

341 The MgO/SiO_2 and Al_2O_3/SiO_2 ratios derived from the 10th January 2009 flare observations are
342 within the range exhibited by mare basalt samples (Figure 6b). The ground track of this flare
343 includes the Apollo 14 landing site, and as such, the C1XS results should have a similar
344 composition to the average soil composition for Apollo 14, which is labelled in Figure 6b. This
345 is indeed the case, with the Apollo 14 soil composition lying within the 1 σ errors of the whole
346 flare ratio and close to the Fra Mauro C1XS data point (although these two points are essentially
347 the same within the errors).
348
349 The discrepancies between the C1XS and Lunar Prospector values observed for the 12th
350 December 2008 flare are also observed for the 10th January 2009 flare (Figure 6b), although
351 perhaps to a lesser extent. This suggests that the validity of comparing these two datasets
352 warrants further investigation and is discussed below in Section 6.4.
353
354 6.3. Variation in spatial scales
355
356 It is possible that the agreement between the Apollo 14 soil sample composition and the C1XS
357 derived MgO/SiO_2 and Al_2O_3/SiO_2 ratios is merely coincidental, owing to the disparity in the
358 spatial scales represented by the soil samples (<0.8 km^2) and the C1XS footprint (~20,000 km^2).
359 This is also true in the case of relating Lunar Prospector gamma-ray data and the soil samples.
360 FeO and TiO_2 concentrations derived from Clementine multispectral reflectance data can be used
361 to investigate this issue. The concentrations derived (using the algorithms of Gillis et al., 2003;
362 2004) for pixels containing only the immediate area around the Apollo 14 site and the Fra Mauro
363 region sampled by C1XS (i.e., within the dashed lines in Figure 3) are similar (within 1 wt. %).
364 The Apollo 14 site concentration and the actual soil data (reported by McKay et al., 1991 and
365 references therein) are equal in terms of TiO_2, but differ by ~3 wt. % in terms of FeO. The
366 expected variation in compositions derived from remotely sensed data at different spatial scales
367 is therefore apparent to some extent in the Clementine data. Fe and Ti were not observed in the
368 C1XS data reported here, so a direct comparison is not possible. We merely not that
369 compositional variations on the order of a few wt. % between the local (sample) scale and the
370 orbital remote sensing measurements are not unexpected.
371

372 6.4. Planetary XRF vs. gamma-ray spectroscopy
373
374 As outlined in Section 6.1, the lack of agreement between the C1XS results presented in this
375 paper and the corresponding Lunar Prospector gamma-ray compositions (especially in terms of
376 MgO/SiO_2) could be due to a combination of factors. Given (i) that the abundance algorithm
377 methodology used here has been proven using laboratory test data from a lunar regolith simulant
378 (Weider et al., 2011); (ii) the agreement of the 10th January 2009 result and the ground truth
379 Apollo 14 sample composition; and (iii) that the errors associated with the uncertain solar flare
380 temperatures are much larger than the algorithm's fitting errors, it is thought that the lack of
381 agreement between the C1XS and Lunar Prospector results is unlikely to be due to the
382 inaccuracy of the C1XS abundances presented here.
383
384 The better agreement between the sample and C1XS data than between the C1XS and Lunar
385 Prospector data, or indeed than between the sample and Lunar Prospector data, further suggest
386 that the discrepancy is more likely to lie with the Lunar Prospector values for Mg (at least on
387 such a local scale as this, rather than for the global dataset). It has been noted (e.g., Wöhler et
388 al., 2011), that for the respective landing sites (based on sample compositions compiled by
389 Elphic et al., 2000) and the Lunar Prospector gamma-ray data, the correlation is not always good.
390 This is especially true for Mg and Al, and particularly the former, which is systematically
391 overestimated (by up to ~5 element wt. %) by Lunar Prospector. Furthermore, Lunar Prospector
392 SiO_2 values (as presented by Prettyman et al., 2006) tend to be lower than Apollo soil
393 compositions. If the Lunar Prospector data points in Figure 6 are normalised not to the
394 Prettyman et al., (2006) SiO_2 values for the particular pixel, but to a sample average or the mean
395 global Lunar Prospector value (i.e., ~43 to 45 wt. %), the ratios in terms of both MgO and Al_2O_3
396 become smaller. The Al_2O_3/SiO_2 Lunar Prospector and C1XS values agree better in all cases,
397 but the Lunar Prospector MgO/SiO_2 values remain higher than the C1XS results, within the
398 errors given. These issues with the Lunar Prospector dataset could therefore, at least in part,
399 explain the C1XS-Lunar Prospector discrepancies and also why they are greater for Mg than Al.
400
401 It is also important to discuss the third possibility; that the discrepancies arise due to intrinsic
402 differences between the two techniques, rather than because of either dataset having inherent

403 inaccuracies. The difference in energy of the radiation measured by the two techniques means
404 that XRF only samples the top 100 microns of the lunar regolith (Yin et al., 1993), whereas
405 gamma-rays can penetrate to a depth of ~1 m (Prettyman et al., 2006); and also that XRF
406 spectroscopy is subject to matrix effects (e.g., Mantler, 2006). XRF analysis involves
407 attenuation corrections that are dependent on the composition of the target material (e.g., Clark
408 and Trombka, 1997); such attenuation corrections are not required for gamma-rays above 1 MeV
409 for the compositional range of lunar materials (Prettyman et al., 2006).
410
411 The different sampling depths of the techniques may mean that compositionally distinct parts of
412 the regolith are measured, with XRF "seeing" only the finest fraction of the soil at the very
413 surface (up to ~100 μm), and gamma-rays seeing a greater mixture, down to a depth of ~1 m.
414 The study of lunar regolith cores that were obtained during the Apollo missions have revealed an
415 uppermost reworked, layer that varies between ~10 cm and ~50 cm deep. Beneath this layer are
416 more complex facies consisting of layers of ejecta material from both large and small craters
417 (McKay et al., 1991). It is therefore possible that the geochemistry of the very top of the regolith
418 measured by XRF is different from the bulk composition of the top 1 m. In addition, regolith
419 grain sorting processes (e.g., seismic shaking; Ostrach and Robinson, 2010) may be able to
420 stratify the regolith and produce compositional layering, at least at in the uppermost layers
421 observed here. The possible importance of such effects on the interpretation of lunar XRF
422 spectroscopy has also been noted by Narendranath et al. (2011). Similar effects have been
423 proposed by Riner et al. (2008) to explain the significantly higher Fe/Si ratios determined from
424 the XRS on NEAR for the asteroid Eros (Lim and Nittler, 2009) than those determined from the
425 GRS. Such compositional layering may also help explain the discrepancies between FeO and
426 TiO_2 concentrations derived from the Lunar Prospector gamma-ray and Clementine multispectral
427 reflectance datasets that have previously been noted (e.g., Lucey et al., 2006).
428
429 An alternative explanation for possible compositional stratification may be the presence of
430 impact-formed, amorphous and inclusion-rich rims (60 – 200 nm thick) on the surface of
431 individual soil grains (e.g., Keller and McKay, 1997). These are thought to be one of the main
432 causes of spectral darkening due to space weathering in reflectance spectroscopy (Pieters et al.,
433 1993; Allen et al., 1996; Keller and McKay, 1997). However, any compositional anomalies in

these very thin rims (even in terms of the ten to hundred micron scale to which XRF spectroscopy is sensitive) are unlikely to play a significant role in affecting the C1XS results.

Clearly, the issue of comparing planetary XRF and gamma-ray spectroscopy results is an important one that warrants further investigation. This should soon be possible through comparisons of C1XS data with the new gamma-ray results from the Kaguya mission (e.g., Gasnault et al., 2009).

7. Conclusions

XRF data obtained by C1XS during two A-class solar flares early in the mission have been analysed in this paper. The ground tracks of the observations pass through: (i) Mare Serenitatis and (ii) Mare Insularum, Mare Cognitum and Mare Nubium, including the Apollo 14 landing site in the Fra Mauro Formation. The calibrated, gain-corrected and background subtracted X-ray spectra for these flares have been fitted using an abundance algorithm in order to provide estimates of the MgO/SiO_2 and Al_2O_3/SiO_2 ratios for the two separate regions. The results agree, within the 1 σ errors, with existing lunar sample compositions and the Apollo 14 average soil composition has been replicated with the flare data that includes this landing site. This represents an independent measure of lunar elemental abundances that can be compared to, but not calibrated with, ground-truth sample data (unlike other lunar remote sensing datasets).

There is, however, some discrepancy between our results and compositions derived from Lunar Prospector gamma-ray data and we suggest that the validity of comparing planetary XRF and gamma-ray spectroscopy results be investigated in more detail. This is especially important for other planetary bodies where no ground truth sample data are available. Examples include Eros (which has already been studied using these techniques; Nittler et al., 2001), and Mercury (with the forthcoming XRS and GRS datasets from MESSENGER (Goldsten et al., 2007; Schlemm et al., 2007) and BepiColombo (Fraser et al., 2010; Rothery et al., 2010). The C1XS-Lunar Prospector discrepancies may be evidence of compositional layering in the uppermost metre of the lunar regolith, where the finest fraction of the soil is compositionally distinct from the bulk material at depth.

The C1XS spectra from the Fra Mauro Formation include a possible detection of Na. When modelled this peak provides a Na abundance estimate that is consistent with the Apollo 14 average soil composition (the most Na-rich of the lunar soils). However due to uncertainties in the solar spectrum at this energy and the inability to separate the contributions from scattered solar lines and XRF from the lunar surface, this result is not presented with confidence.

While this paper documents the first solar flare events observed by the C1XS instrument, the data yield for just Mg and Al, is relatively small. Other results (e.g., Narendranath et al., 2011) from higher energy events illustrate better the full power (including data for Ca and Fe) of the C1XS instrument and XRF spectroscopy for the Moon and other suitable solar system bodies.

8. Acknowledgements

The authors thank an anonymous reviewer and Tom Prettyman for their helpful and thoughtful comments that have served to significantly improve this manuscript. C1XS was an ESA-provided instrument on India's Chandrayaan-1 spacecraft. We thank ESA and ISRO for this collaborative opportunity, and for support in mission planning, spacecraft operations, and data processing and archiving. SZW, KHJ and IAC acknowledge STFC and the Leverhulme Trust for financial support. This is LPI contribution ****.

9. References

Adler, I., Trombka, J.I., 1977. Orbital chemistry – lunar surface analysis from the X-ray and gamma ray remote sensing experiments. Phys. Chem. Earth 10, 17-43.

Adler, I., Trombka, J., Gerard, J., Lowman, P., Schmadebeck, R., Blodget, H., Eller, E., Yin, L., Lamothe, R., Gorenstein, P., Bjorkholm, P., 1972a. Apollo 15 geochemical X-ray fluorescence experiment: preliminary report. Science 175, 436-440.

Adler, I., Trombka, J., Gerard, J., Lowman, P., Schmadebeck, R., Blodget, H., Eller, E., Yin, L., Lamothe, R., Osswald, G., Gorenstein, P., Bjorkholm, P., Gursky, H., Harris, B., 1972b. Apollo 16 geochemical X-ray fluorescence experiment: preliminary report. Science 177, 256-259.

Alha, L., Huovelin, J., Hackman, T., Andersson, H., Howe, C.J., Esko, E., Väänänen, M., 2008. The in-flight performance of the X-ray solar monitor (XSM) on-board SMART-1. Nucl. Instrum. Methods in Phys. Res., A 596, 317-326.

Alha, L., Huovelin, J., Nygård, K., Andersson, H., Esko, E., Howe, C.J., Kellett, B.J., Narendaranth, S., Maddison, B.J., Crawford, I.A., Grande, M., Sreekumar, P., 2009. Ground calibration of the Chandrayaan-1 X-ray Solar Monitor (XSM). Nucl. Instrum. Methods in Phys. Res., A 607, 544-553.

Allen, C.C., Morris, R.V., McKay, D.S., 1996. An experimental analog to maturing lunar soil. Proc. Lunar Planet. Sci. Conf. 27th, 13-14.

Andre, C.G., Bielefeld, M.J., Eliason, E., Soderblom, L.A., Adler, I., Philpotts, J.A., 1977. Lunar surface geochemistry: a new imaging technique. Science 197, 986-989.

Belton, M.J.S., Greeley, R., Greenberg, R., McEwen, A., Klaasen, K.P., Head, J.W., III, Pieters, C., Neukum, G., Chapman, C.R., Geissler, P., Heffernan, C., Breneman H., Anger, C., Carr, M.H., Davies, M.E., Fanale, F.P., Gierasch, P.J., Ingersoll, A.P., Johnson, T.V., Pilcher, C.B., Thompson, W.R., Veverka, J., Sagan, C., 1994. Galileo multispectral imaging of the north polar and eastern limb regions of the Moon. Science 264, 1112-1115.

Bhandari, N., 2005. Chandrayaan-1: science goals. J. Earth Syst. Sci. 114, 701-709.

Bouwer, S.D., 1983. Intermediate-term epochs in solar soft X-ray emission. J. Geophys. Res. 88 (A10), 7823-2830.

525 Clark, P.E., Trombka, J.I., 1997. Remote X-ray spectrometry for NEAR and future missions:
526 modeling and analyzing X-ray production from source to surface. J. Geophys. Res. 102, 16,361-
527 16,384.
528
529 Crawford, I.A., Joy, K.H., Kellett, B.J., Grande, M., Anand, M., Bhandari, N., Cook, A.C.,
530 d'Uston, L., Fernandes, V.A., Gasnault, O., Goswami, J., Howe, C.J., Huovelin, J., Koschny, D.,
531 Lawrence, D.J., Maddison, B.J., Maurice, S., Narendranath, S., Pieters, C., Okada, T., Rothery,
532 D.A., Russell, S.S., Sreekumar, P., Swinyard, B., Wieczorek, M., Wilding, M., 2009. The
533 scientific rationale for the C1XS X-ray Spectrometer on India's Chandrayaan-1 mission to the
534 Moon. Planet. Space Sci. 57, 725-734.
535
536 Crosby, N.B., Aschwanden, M.J., Dennis, B.R., 1993. Frequency distribution and correlations of
537 solar X-ray flare parameters. Sol. Phys. 143, 275-299.
538
539 Donnelly, R.F., 1976. Empirical models of solar flare X-ray and EUV emission for use in
540 studying their E and F region effects. J. Geophys. Res. 81, 4745-4753.
541
542 Elphic, R.C., Lawrence, D.J., Feldman, W.C., Barraclough, B.L., Maurice, S, Binder, A.B.,
543 Lucey, P.G., 2000. Lunar and rare earth element distribution and ramifications for FeO and
544 TiO_2: Lunar Prospector neutron spectrometer observations. J. Geophys. Res. 105 (E8), 20,333-
545 20,345.
546
547 Fraser, G.W., Carpenter, J.D., Rothery, D.A., Pearson, J.F., Martindale, A., Huovelin, J., Treis,
548 J., Anand, M., Anttila, M., Ashcroft, M., Benkoff, J., Bland, P., Bowyer, A., Bradley, A.,
549 Bridges, J., Brown, C., Bulloch, C., Bunce, E.J., Christensen, U., Evans, M., Fairbend, R.,
550 Feasey, M., Giannini, F., Hermann, S., Hesse, M., Hilchenbach, M., Jorden, T., Joy, K.,
551 Kaipiainen, M., Kitchingman, I., Lechner, P., Lutz, G., Malkki, A., Muinonen, K., Näränen, J.,
552 Portin, P., Prydderch, M., San Juan, J., Sclater, E., Schyns, E., Stevenson, T.J., Strüder, L.,
553 Syrjasuo, M., Talboys, D., Thomas, P., Whitford, C., Whitehead, S., 2010. The mercury imaging
554 X-ray spectrometer (MIXS) on bepicolombo. Planet. Space Sci. 58, 79-95.
555

Fruland, R.M., 1983. Regolith breccia workbook, JSC 19045. NASA Johnson Space Center, Houston.

Gasnault, O., Forni, O., Diez, B., d'Uston, C., Hasebe, N., Okudaira, O., Yamashita, N., Kobayashi, S., Karouji, Y., Hareyama, M., Shibamura, E., Kobayashi, M.N., Reedy, R.C., the Selene GRS team, 2009. Preliminary analysis of SELENE GRS data – the iron case. Proc. Lunar Planet. Sci. Conf. 40th, abstract #2253.

Gillis, J.J., Jolliff, B.L., Elphic, R.C., 2003. A revised algorithm for calculating TiO_2 from Clementine UVVIS data: a synthesis of rock, soil, and remotely sensed TiO_2 concentrations. J. Geophys. Res. 108 (E2), 5009, doi: 10.1029/2001JE001515.

Gillis, J.J., Jolliff, B.L., Korotev, R.L., 2004. Lunar surface geochemistry: global concentrations of Th, K, and FeO as derived from Lunar Prospector and Clementine data. Geochim. Cosmochim. Acta 68, 3791-3805.

Glotch, T.D., Lucey, P.G., Bandfield, J.L., Greenhagen, B.T., Thomas, I.R., Elphic, R.C., Bowles, N., Wyatt, M.B., Allen, C.C., Donaldson Hanna, K., Paige, D.A., 2010. Highly silicic compositions on the Moon. Science 329, 1510-1513.

Goldsten, J.O., Rhodes, E.A., Boynton, W.V., Feldman, W.C., Lawrence, D.J., Trombka, J.I., Smith, D.M., Evans, L.G., White, J., Madden, N.W., Berg, P.C., Murhpy, G.A., Gurnee, R.S., Strohbehn, K., Williams, B.D., Schaefer, E.D., Monaco, C.A., Cork, C.P., Del Eckels, J., Miller, W.O., Burks, M.T., Hagler, L.B., DeTeresa, S.J., Witte, M.C., 2007. The MESSENGER gamma-ray and neutron spectrometer. Space Sci. Rev. 131, 339-391.

Goswami, J.N., Annadurai, 2009. Chandrayaan-1: India's first planetary science mission to the Moon. Current Sci. 96, 486-491.

Grande, M., Browning, R., Waltham, N., Parker, D., Dunkin, S.K., Kent, B., Kellett, B., Perry, C.H., Swinyard, B., Perry, A., Feraday, J., Howe, C., McBride, G., Phillips, K., Huovelin, J.,

587 Muhli, P., Hakala, P.J., Vilhu, O., Laukkanen, J., Thomas, N., Hughes, D., Alleyne, H., Grady,
588 M., Lundin, R., Barabash, S., Baker, D., Clark, P.E., Murray, C.D., Guest, J., Casanova, I.,
589 d'Uston, L.C., Maurice, S., Foing, B., Heather, D.J., Fernandes, V., Muinonen, K., Russell, S.S.,
590 Christou, A., Owen, C., Charles, P., Koskinen, H., Kato, M., Sipila, K., Nenonen, S., Holmstrom,
591 M., Bhandari, N., Elphic R., Lawrence, D., 2003. The D-CIXS X-ray mapping spectrometer on
592 SMART-1. Planet. Space Sci. 51, 427-433.
593
594 Grande, M., Kellett, B.J., Howe, C., Perry, C.H., Swinyard, B., Dunkin, S.., Huovelin, J., Alha,
595 L., D'Uston, L.C., Maurice, S., Gasnault, O., Couturier-Doux, S., Barabash, S., Joy, K.H.,
596 Crawford, I.A., Lawrence, D., Fernandes, V., Casanova, I., Wieczorek, M., Thomas, N., Mall,
597 U., Foing, B., Hughes, D., Alleyne, H., Russell, S., Grady, M., Lundin, R., Baker, D., Murray,
598 C.D., Guest, J., Chrsitou, A., 2007. The D-CIXS X-ray spectrometer on the SMART-1 mission
599 to the Moon – first results. Planet. Space Sci. 55, 494-502.
600
601 Grande, M., Maddison, B.J., Howe, C.J., Kellett, B.J., Sreekumar, P., Huovelin, J., Crawford,
602 I.A., d'Uston, C.L., Smith, D., Anand, M., Bhandari, N., Cook, A., Fernandes, V., Foing, B.,
603 Gasnault, O., Goswami, J.N., Holland, A., Joy, K.H., Kochney, D, Lawrence, D., Maurice, S.,
604 Okada, T., Narendranath, S., Pieters, C., Rothery, D, Russell, S.S., Shrivastava, A., Swinyard, B.,
605 Wilding, M., Wieczorek, M., 2009a. The C1XS X-ray spectrometer on Chandrayaan-1. Planet.
606 Space Sci. 57, 717-724.
607
608 Grande, M., Maddison, B.J., Sreekumar, P., Huovelin, J., Kellett, B.J., Howe, C.J., Crawford,
609 I.A., Smith, D.R., the C1XS team, 2009b. The Chandrayaan-1 X-ray spectrometer. Current Sci.
610 96, 517-519.
611
612 Greenhagen, B.T., Lucey, P.G., Wyatt, M.B., Glotch, T.D., Allen, C.C., Arnold, J.A., Bandfield,
613 J.L., Bowles, N.E., Donaldson Hanna, K.L., Hayne, P.O., Song, E., Thomas, I.R., Paige, D.A.,
614 2010. Global silicate mineralogy of the Moon from the Diviner Lunar Radiometer. Science 329,
615 1507-1509.
616

617 Haskin, L.A., Korotev, R.L., Gillis, J.J., Jolliff, B.L., 2002. Stratigraphies of Apollo and Luna
618 highland landing sites and provenances of materials from the perspective of basin impact ejecta
619 modeling. Proc. Lunar Planet. Sci. Conf. 33rd, abstract #1364.
620
621 He, F., Van Espen, P.J., 1991. General approach for quantitative energy dispersive X-ray
622 fluorescence analysis based on fundamental parameters. Anal. Chem. 63, 2237-2244.
623
624 Hiesinger, H., Head, J.W., III, 2006. New views of lunar geoscience: an introduction and
625 overview. Rev. Min. Geochem. 60, 1-81.
626
627 Hiesinger, H., Head, J.W., III, Wolf, U., Jaumann, R., Neukum, G., 2003. Ages and stratigraphy
628 of mare basalts in Oceanus Procellarum, Mare Nubium, Mare Cognitum, and Mare Insularum. J.
629 Geophys. Res. 108 (E7), 5065, doi: 10.1029/2002JE001985.
630
631 Hiesinger, H., Jaumann, R., Neukum, G., Head, J.W., III, 2000. Ages of mare basalts on the
632 lunar nearside. J. Geophys. Res. 105 (E12), 29,239-29,275.
633
634 Holland, A.D., Hutchinson, I.B., Smith, D.R., Pool, P., 2004. Proton damage in the E2V swept
635 charge device. Nucl. Instrum. Methods Phys. Res., A 521, 393-398.
636
637 Howe, C.J., Drummond, D., Edeson, R., Maddison, B, Parker, D.J., Parker, R., Shrivastava, A.,
638 Spencer, J., Kellett, B.J., Grande, M., Sreekumar, P., Huovelin, J., Smith, D.R., Gow, J.,
639 Narendranath, S., d'Uston, L., 2009. Chandrayaan-1 X-ray Spectrometer (C1XS) - instrument
640 design and technical details. Planet. Space Sci. 57, 735-743.
641
642 Huovelin, J., Alha, L., Andersson, H., Andersson, T., Browning, R., Drummond, D., Foing, B.,
643 Grande, M., Hämäläinen, ., Laukkanen, J., Lämsä, V., Muinonen, K., Murray, M., Nenonen, S.,
644 Salminen, A., Sipilä, H., Taylor, I., Vilhu, O., Waltham, N., Lopez-Jorkama, M., 2002. The
645 SMART-1 X-ray solar monitor (XSM): calibrations for D-CIXS and independent coronal
646 science. Planet. Space Sci. 50, 1345-1353.
647

Jerde, E.A., Morris, R.V., Warren, P.H., 1990. In quest of lunar regolith breccias of exotic provenance: a uniquely anorthositic sample from the Fra Mauro (Apollo 14) highlands. Earth Planet. Sci. Lett. 98, 90-108.

Jerde, E.A., Warren, P.H., Morris, R.V., Heiken, G.H., Vaniman, D.T., 1987. A potpourri of regolith breccias: "new" samples from the Apollo 14, 16 and 17 landing sites. Proc. Lunar Planet. Sci. Conf. 17th, J. of Geophys. Res. 92 (B4), E526-E536.

Jolliff, B.L., Gillis, J.J., Haskin, L.A., Korotev, R.L., Wieczorek, M.A., 2000. Major lunar crustal terranes: surface expressions and crust-mantle origins. J. Geophys. Res. 105 (E2), 4197-4216.

Kay, H.R.M., Harra, L.K., Matthews, S.A., Culhane, J.L., Green, L.M., 2003. The soft X-ray characteristics of solar flares, both width and without associated CMEs. Astron. Astrophys. 400, 779-784.

Keller, L.P., McKay, D.S., 1997. The nature and origin of rims on lunar soil grains. Geochim. Cosmochim. Acta 61, 2331-2341.

Lawrence, D.J., Elphic, R.C., Feldman, W.C., Prettyman, T.H., Gasnault, O., Maurice, S., 2003. Small-area thorium features on the lunar surface. J. Geophys. Res. 108 (E9), 5102, doi: 10.1029/2003JE002050.

Lawrence, D.J., Feldman, W.C., Elphic, R.C., Little, R.C., Prettyman, T.H., Maurice, S., Lucey, P.G., Binder, A.B., 2002. Iron abundances on the lunar surface as measured by the Lunar Prospector gamma-ray and neutron spectrometers. J. Geophys. Res. 107 (E12), 5130, doi: 10.1029/2001JE001530.

Lim, L.F., Nittler, L.R., 2009. Elemental composition of 433 Eros: new calibration of the NEAR-Shoemaker XRS data. Icarus 200, 129-146.

679 Lucey, P.G., 2004. Mineral maps of the Moon. Geophys. Res. Lett. 31, L08701,
680 doi: 10.1029/2003GL019406.
681
682 Lucey, P.G., Blewett, D.T., Hawke, B.R., 1998. Mapping the FeO and TiO_2 content of the lunar
683 surface with multispectral imagery. J. Geophys. Res. 103 (E2), 3679-3699.
684
685 Lucey, P.G., Blewett, D.T., Jolliff, B.L., 2000. Lunar iron and titanium abundance algorithms
686 based on final processing of Clementine ultraviolet-visible images. J. Geophys. Res. 105 (E8),
687 20,297-20,305.
688
689 Lucey, P.G., Cahill, J., 2006. Magnesian rock types in the lunar highlands: remote sensing using
690 data from Lunar Prospector and Clementine. Proc. Lunar Planet, Sci. Conf. 37th, abstract #1660.
691
692 Lucey, P., Korotev, R.L., Gillis, J.J., Taylor, L.A., Lawrence, D., Campbell, B.A., Elphic, R.,
693 Feldmann, B., Hood, L.L., Hunten, D., Mendillo, M., Noble, S., Papike, J.J., Reedy, R.C.,
694 Lawson, S., Prettyman, T., Gasnault, O., Maurice, S., 2006. Understanding the lunar surface and
695 space-moon interactions. Rev. Mineral. Geochem. 60, 83-219.
696
697 Mantler, M., 2006. Quantitative analysis, in: Beckhoff, B., Kanngießer, B., Langhoff, N.,
698 Wedell, R., Wolff, H. (Eds), Practical X-ray fluorescence analysis. Springer, pp. 309-410.
699
700 Maruyama, Y., Ogawa, K., Okada, T., Kato, M., 2008. Laboratory experiments of particle size
701 effect in X-ray fluorescence and implications to remote X-ray spectrometry of lunar regolith
702 surface. Earth Planets Space 60, 293-297.
703
704 McKay, D.S., Bogard, D.D., Morris, R.V., Korotev, R.L., Johnson, P., Wentworth, S.J., 1986.
705 Apollo 16 regolith breccias: characterization and evidence for early formation in the mega-
706 regolith. Proc. Lunar Planet. Sci. Conf. 16th, J. Geophys. Res. 91 (B4), D277-D303.
707

McKay, D.S., Bogard, D.D., Morris, R.V., Korotev, R.L., Wentworth, S.J., Johnson, P., 1989. Apollo 15 regolith breccias: window to a KREEP regolith. Proc. Lunar Planet. Sci. Conf. 19th, 19-41.

McKay, D.S., Heiken, G., Basu, A., Blanford, G., Simon, S., Reedy, R., French, B.M., Papike, J., 1991. The lunar regolith, in: Heiken, G.H., Vaniman, D.T., French, B.M. (Eds), Lunar Sourcebook: a user's guide to the Moon. Cambridge University Press, pp. 285-356.

Morris, R.V., Score, R., Dardano, C., Heiken, G., 1983. Handbook of lunar soils, JSC 19069. NASA Johnson Space Center, Houston.

Morrison, R.H., Oberbeck, V.R., 1975. Geomorphology of crater and basin deposits – emplacement of the Fra Mauro Formation. Proc. Lunar Sci. Conf. 6th, 2503-2530.

Näränen, J., Parviainen, H., Muinonen, K., Carpenter, J., Nygård, K., Peura, M., 2008. Laboratory studies into the effect of regolith on planetary X-ray fluorescence spectroscopy. Icarus 198, 408-419.

Narendranath, S., Athiray, P.S., Sreekumar, P., Kellett, B.J., Alha, L., Howe, C.J., Joy, K.H., Grande, M., Huovelin, J., Crawford, I.A., Unnikrishnan, U., Lalita, S., Subramaniam, S., Weider, S.Z., Nittler, L.R., Gasnault, O., Rothery, D., Fernandes, V.A., Bhandari, N., Goswami, J.N., Wieczorek, M.A., the C1XS team, 2011. Lunar X-ray fluorescence observations by the Chandrayaan-1 X-ray Spectrometer (C1XS): results from the nearside southern highlands. Icarus 214, 53-66.

Narendranath, S., Athiray, P.S., Unnikrishnan, U., Sreekumar, P., the C1XS team, 2010b. Analysis of lunar X-ray data: line flux to elemental abundance from the C1XS experiment on Chandrayaan-1. Proc. X-ray Fluoresc. Spectrosc. in Planet. Remote Sens. Workshop, ESA SP-687.

738 Narendranath et al., S., Sreekumar, P., Maddison, B.J., Howe, C.J., Kellett, B.J., Wallner, M.,
739 Erd, C., Weider, S.Z., 2010a. Calibration of the C1XS instrument on Chandrayaan-1. Nucl.
740 Instrum. Methods Phys. Res., A 621, 344-353.
741
742 Nittler, L. R., Starr, R. D., Lim, L., McCoy, T. J., Burbine, T. H., Reedy, R. C., Trombka, J. I.,
743 Gorenstein, P., Squyres, S. W., Boynton, W. V., McClanahan, T. P., Bhangoo, J. S., Clark, P. E.,
744 Murphy, M. E., Killen, R., 2001. X-ray fluorescence measurements of the surface elemental
745 composition of asteroid 433 Eros, Meteoritic. Planet. Sci. 36, 1673-1695.
746
747 Ostrach, L.R., Robinson, M.S., 2010. Effects of seismic shaking on grain size and density
748 sorting with implications for constraining lunar bulk regolith composition. Proc. Lunar Planet,
749 Sci. Conf. 41, abstract #2521.
750
751 Papike, J.J., Ryder, G., Shearer, C.K., 1998. Lunar samples. Rev. Mineral. 36, 5.1-5.234.
752
753 Pieters, C.M., Fischer, E.M., Rode, O., Basu, A., 1993. Optical effects of space weathering: the
754 role of the finest fraction. J. Geophys. Res. 98 (E11), 20,817-20,824.
755
756 Pieters, C.M., Tompkins, S., 1999. Tsiolkovsky crater: a window into crustal processes on the
757 lunar farside. J. Geophys. Res. 104 (E9), 21,935-21,949.
758
759 Pieters, C., Shkuratov, Y., Kaydash, V., Stankevich, D., Taylor, L., 2006. Lunar soil
760 characterization consortium analyses: pyroxene and maturity estimates derived from Clementine
761 image data. Icarus 184, 83-101.
762
763 Prettyman, T.H., Hagerty, J.J., Elphic, R.C., Feldman, W.C., Lawrence, D.J., McKinney, G.W.,
764 Vaniman, D.T., 2006. Elemental composition of the lunar surface: analysis of gamma ray
765 spectroscopy data from Lunar Prospector. J. Geophys. Res. 111, E12007,
766 doi: 10.1029/2005JE002656.
767

768 Rhodes, J.M., Blanchard, D.P., 1981. Apollo 11 breccias and soils: aluminous mare basalts or
769 multi-component mixtures? Proc. Lunar Planet. Sci. Conf. 12th, 607-620.
770
771 Riner, M.A., Robinson, M.S., Eckart, J.M., Desch, S.J., 2008. Global survey of color variations
772 on 433 Eros: implications for regolith processes and asteroid environments. Icarus 198, 67-76.
773
774 Rothery, D.A., Marinangeli, L., Anand, M., Carpenter, J., Christensen, U., Crawford, I.A.,
775 Sanctis, M.C., Epifani, E.M., Erard, S., Frigeri, A., Fraser, G., Hauber, E., Helbert, J., Hiesinger,
776 H., Joy, K.H., Langevin, Y., Massironi, M., Milillo, A., Mitrofanov, I., Muinonen, K., Näränen,
777 J., Pauselli, C., Potts, P., Warell, J., Wurz, P., 2010. Mercury's surface and composition to be
778 studied by BepiColombo. Planet. Space Sci. 58, 21-39.
779
780 Schlemm, C.E., II., Starr, R.D., Ho, G.C., Bechtold, K.E., Hamilton, S.A., Boldt, J.D., Boynton,
781 W.V., Bradley, W., Fraeman, M.E., Gold, R.E., Goldsten, J.O., Hayes, J.R., Jaskulek, S.E.,
782 Rossano, E., Rumpf, R.A., Schaefer, E.D., Strohbehn, K., Shelton, R.G., Thompson, R.E.,
783 Trombka, J.E., Williams, B.D., 2007. The X-ray spectrometer on the MESSENGER spacecraft.
784 Space Sci. Rev. 131, 393-415.
785
786 Shearer, C.K., Hess, P.C., Wieczorek, M.A., Pritchard, M.E., Parmentier, E.M., Borg, L.E.,
787 Longhi, J., Elkins-Tanton, L.T., Neal, C.R., Antonenko, I., Canup, R.M., Halliday, A.N., Grove,
788 T.L., Hager, B.H., Lee, D.-C., Wiechert, U., 2006. Thermal and magmatic evolution of the
789 Moon. Rev. Mineral. Geochem. 60, 365-518.
790
791 Simon, S.B., Papike, J.J., Gosselin, D.C., Laul, J.C., 1985. Petrology and chemistry of Apollo 12
792 regolith breccias. Proc. Lunar Planet. Sci. Conf. 16th, J. Geophys. Res. 90, D75-D86.
793
794 Smith, D.R., Gow, J., 2009. The effect of protons on the performances of swept-charge devices.
795 Nucl. Instrum. Methods Phys. Res., A 604, 177-179.
796

797 Smith, D.R., Gow, J., Holland, A.D., 2007. Proton irradiation of swept-charge devices for the
798 Chandrayaan-1 X-ray Spectrometer (C1XS). Nucl. Instrum. Methods Physics Res., A 583, 270-
799 277.
800
801 Stadermann, F.J., Heusser, E., Jessberger, E.K., Lingner, S., Stöffler, D., 1991. The case for a
802 younger Imbrium basin: new ^{40}Ar-^{39}Ar ages of Apollo 14 rocks. Geochim. Cosmochim. Acta
803 55, 2339-2349.
804
805 Stöffler, D., Bobe, K.D., Jessberger, E.K., Linger, S., Palme, H., Spettel, B., Stadermann, F.,
806 Wänke, H., 1989. Fra Mauro Formation, Apollo 14: IV. Synopsis and synthesis of consortium
807 studies, in: Taylor, G.J., Warren, P.H. (Eds), Workshop on Moon in Transition: Apollo 14,
808 KREEP, and evolved lunar rocks. LPI Tech. Rep. 89-3, 145-148.
809
810 Stöffler, D., Ryder, G., Ivanov, B.A., Artemieva, N.A., Cintala, M.J., Grieve, R.A.F., 2006.
811 Cratering history and lunar chronology. Rev. Mineral. Geochem. 60, 519-596.
812
813 Swinyard, B.M., Joy, K.H., Kellett, B.J., Crawford, I.A., Grande, M., Howe, C.J., Fernandes,
814 V.A., Gasnault, O., Lawrence, D.J., Russell, S.S., Wieczorek, M.A., Foing, B.H., and the
815 SMART-1 team, 2009. X-ray fluorescence observations of the Moon by SMART-1/D-CIXS and
816 the first detection of Ti K_α from the lunar surface. Planet. Space Sci. 57, 744-750.
817
818 Swinyard, B., Kellett, B., Weider, S., Joy, K.H., Crawford, I.A., and the C1XS team, 2010.
819 C1XS spectral analysis method. Proc. X-ray Fluoresc. Spectrosc. in Planet. Remote Sens.
820 Workshop, ESA SP-687.
821
822 Taylor, G.J., Warren, P., Ryder, G., Delano, J., Pieters, C., Lofgren, G., 1991. Lunar rocks, in:
823 Heiken, G.H., Vaniman, D.T., French, B.M., (Eds.), Lunar Sourcebook: a user's guide to the
824 Moon. Cambridge University Press, pp. 183-284.
825

826 Weider. S.Z., 2011. Studies in lunar geology using existing remote sensing datasets and new
827 orbital X-ray fluorescence spectroscopy from C1XS on Chandrayaan-1. PhD thesis, Birkbeck
828 College, University of London.
829
830 Weider, S.Z., Swinyard, B.M., Kellett, B.J., Howe, C.J., Joy, K.H., Crawford, I.A., Gow, J.,
831 Smith, D.R., 2011. Planetary X-ray fluorescence analogue laboratory experiments and an
832 elemental abundance algorithm for C1XS. Planet. Space Sci. doi:10.1016/j.pss.2011.05.005.
833
834 Wilhelms, D.E., McCauley, J.F., Trask, N.J., 1987. The geologic history of the Moon, U.S.
835 Geological Survey, Washington D.C.
836
837 Wöhler, C., Berezhnoy, A., Evans, R., 2011. Estimation of elemental abundances of the lunar
838 regolith using Clementine UVVIS+NIR data. Planet. Space Sci. 59, 92-110.
839
840 Yin, L.I., Trombka, J.I., Adler, I., Bielefeld, M., 1993. X-ray remote sensing techniques for
841 geochemical analysis of planetary surfaces, in: Pieters, C.M., Englert, P.A. (Eds), Remote
842 geochemical analysis: elemental and mineralogical composition. Cambridge University Press,
843 pp. 199-212.
844
845

Table 1. Boresight location and phase angle during the December 12th 2008 and 10th January 2009 A-class solar flare C1XS observations.

	12th December 2008				10th January 2009			
	Time (U.T.)	**Boresight longitude (°)**	**Boresight latitude (°)**	**Phase angle (°)**	**Time (U.T.)**	**Boresight longitude (°)**	**Boresight latitude (°)**	**Phase angle (°)**
Start	02:27:00	14.01	44.24	45.17	15:56:00	-17.34	6.92	25.83
End	02:39:00	12.89	8.14	9.63	16:08:00	-18.18	-29.70	37.73

Table 2. Modelled abundances (elemental wt. %) for the lines in the spectra of both flares, with 1 σ fitting errors provided. Values are given for the upper and lower limits adopted for the flare temperatures (here expressed in units of a million kelvin; MK). Oxygen and silicon values are fixed in the modelling at the Lunar Prospector (Prettyman et al., 2006) average lunar surface composition values of 44.00 and 21.00 element wt. % respectively.

	12th December 2008				10th January 2009			
	All		*Mare*		*All*		*Fra Mauro*	
	2.5 MK	**3.1 MK**	**2.5 MK**	**3.1 MK**	**2.5 MK**	**3.1 MK**	**2.5 MK**	**3.1 MK**
Mg	3.00 ± 0.13	4.50 ± 0.13	3.00 ± 0.13	4.50 ± 0.38	4.75 ± 0.13	7.00 ± 0.25	3.75 ± 0.38	5.75 ± 0.63
Al	7.75 ± 0.38	10.00 ± 0.38	5.25 ± 0.88	6.50 ± 1.13	8.00 ± 0.50	10.50± 0.63	7.25 ± 1.13	9.50 ± 1.50

Table 3. Mean MgO/SiO_2 and Al_2O_3/SiO_2 ratios for 12th December 2008 and 10th January 2009 flares, as well as their smaller subsections. These mean values are calculated from the individual modelling of the spectra at both 2.5 MK and 3.1 MK (see Table 2). The errors combine the fitting errors and the range in values incorporated due to the two temperature models. The C1XS values are compared with the Lunar Prospector (L.P.) gamma-ray results (Prettyman et al., 2006) for pixels that overlap with the C1XS regions (as shown in Figure 2 and Figure 3).

	MgO/SiO_2			Al_2O_3/SiO_2		
	C1XS	**L.P. Mean**	**L.P. Values**	**C1XS**	**L.P. Mean**	**L.P. Values**
12th Dec. 2008 Whole flare	0.14 ± 0.03	0.28	0.27 ± 0.03	0.37 ± 0.06	0.40	0.45 ± 0.04
			0.25 ± 0.03			0.36 ± 0.04
			0.28 ± 0.03			0.43 ± 0.03
			0.34 ± 0.03			0.76 ± 0.03
12th Dec. 2008 Mare	0.14 ± 0.04	0.28	0.25 ± 0.03	0.25 ± 0.07	0.29	0.29 ± 0.04
			0.29 ± 0.03			0.29 ± 0.04
			0.31 ± 0.03			0.25 ± 0.04
			0.27 ± 0.03			0.34 ± 0.03
10th Jan. 2009 Whole flare	0.20 ± 0.05	0.27	0.24 ± 0.02	0.36 ± 0.07	0.44	0.44 ± 0.03
			0.22 ± 0.03			0.55 ± 0.03
			0.13 ± 0.03			0.32 ± 0.03
			0.25 ± 0.03			0.39 ± 0.03
			0.33 ± 0.03			0.37 ± 0.03
			0.31 ± 0.03			0.53 ± 0.03
10th Jan. 2009 Fra Mauro	0.16 ± 0.05	0.32	0.33 ± 0.03	0.33 ± 0.10	0.45	0.34 ± 0.03
			0.34 ± 0.03			0.47 ± 0.03
			0.28 ± 0.03			0.54 ± 0.04

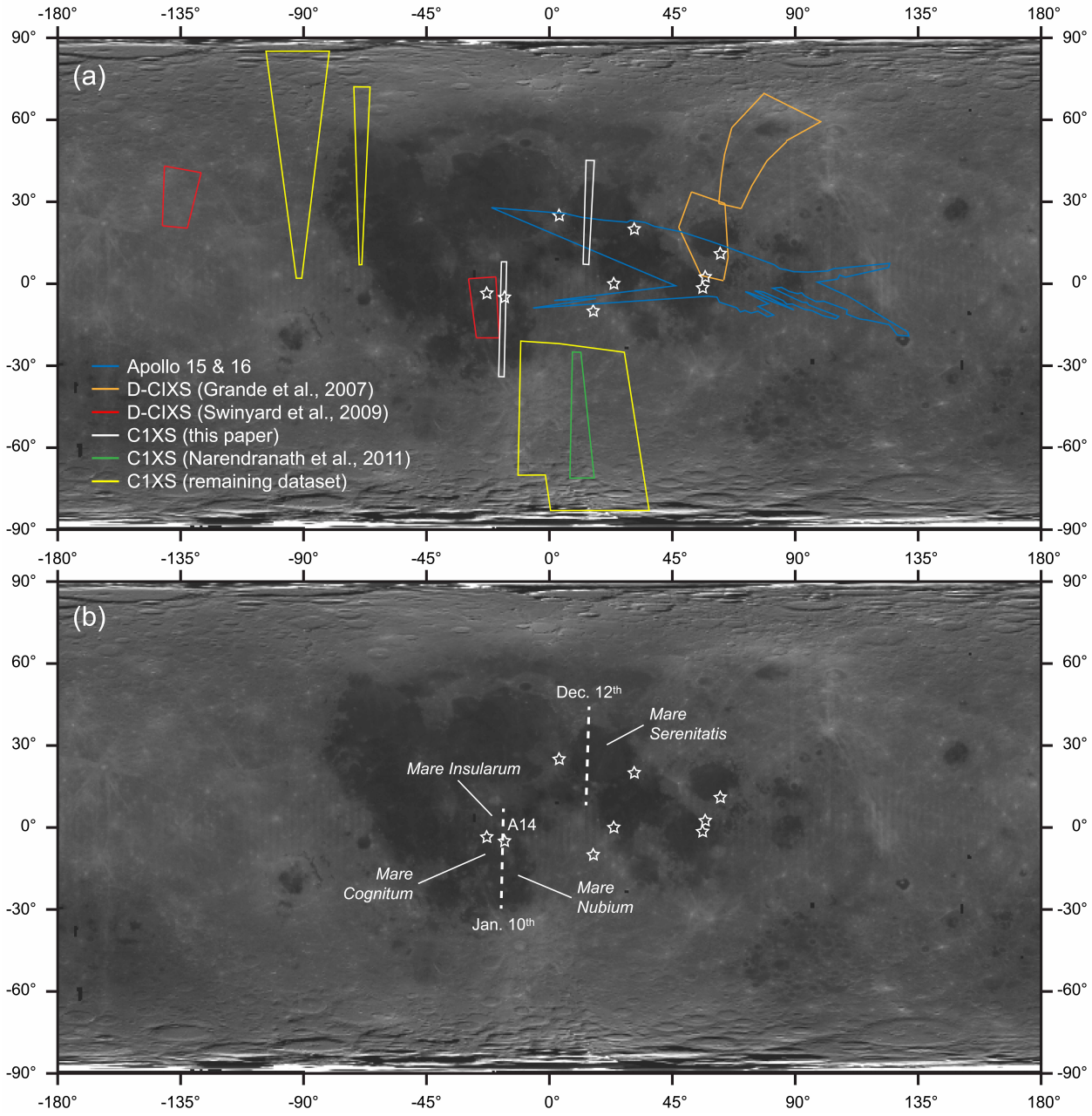

Figure 1. (a) Clementine albedo (750 nm) basemap of the Moon summarising XRF mapping of the lunar surface achieved by the Apollo 15 and 16, D-CIXS and C1XS instruments. All these data provide abundance information for Mg, Al, and Si; in some cases (Grande et al., 2007; Swinyard et al., 2009; Narendranath et al., 2011) other elements (i.e., Ca, Ti and Fe) are also detected. (b) Shows the boresight ground tracks (dashed lines) of the 12th December 2008 and 10th January 2009 C1XS observations, as well as the Apollo and Luna sample return mission landing sites (stars).

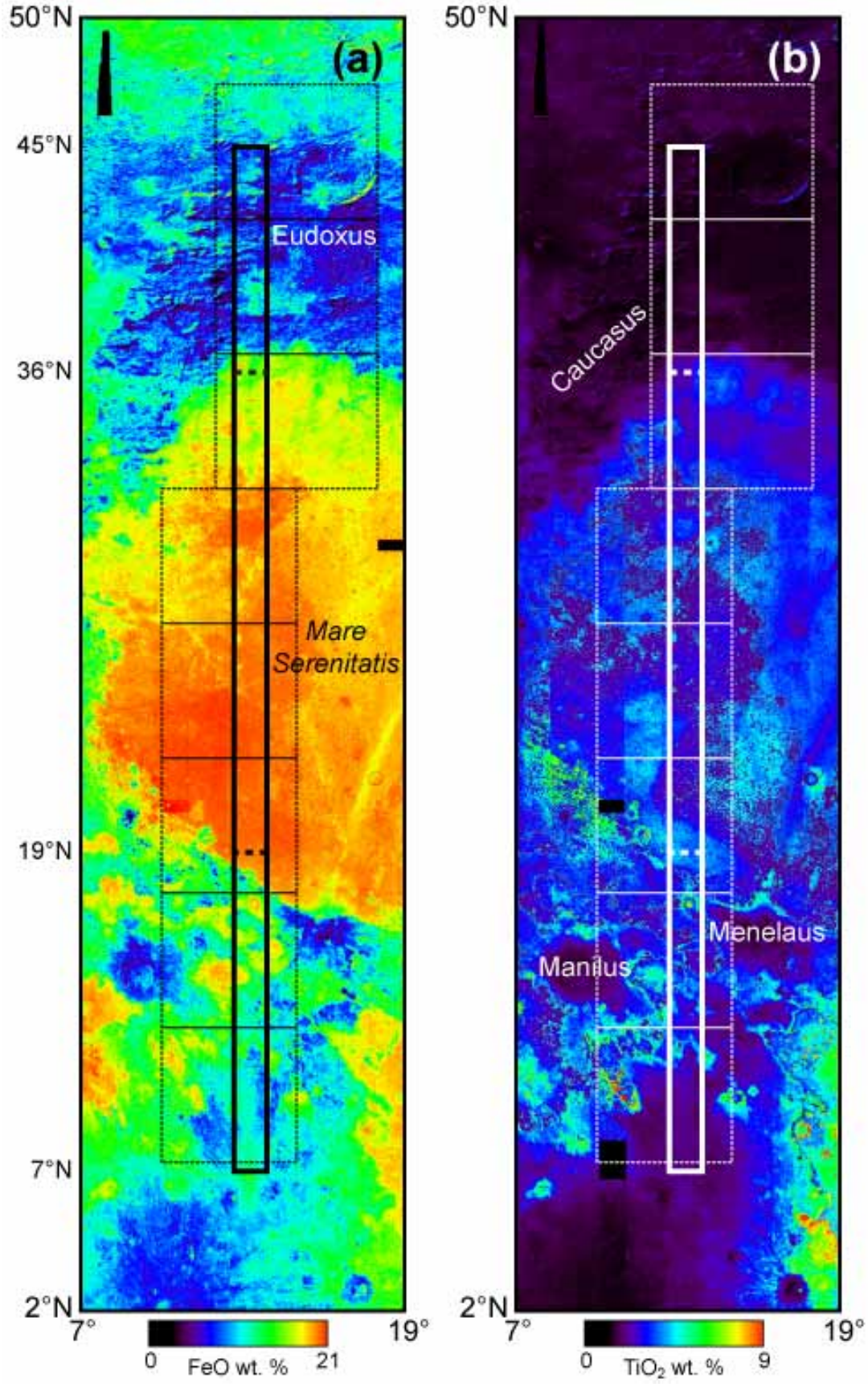
50°N
45°N
36°N
19°N
7°N
2°N
7°
19°
(a)
Eudoxus
Mare
Serenitatis
0
FeO wt. %
21
(b)
Caucasus
Menelaus
Manilus
0
TiO2 wt. %
9

872

873 Figure 2. Maps of: (a) FeO wt. % and (b) TiO_2 wt. % content for the 12th December 2008 flare
874 region, derived from Clementine multispectral reflectance data according to the algorithms of
875 Gillis et al. (2004) and Gillis et al. (2003) respectively. The flare ground track (bold) and the
876 mare subsection (bold dashed lines) are indicated; the width of the outlined boxes corresponds to
877 the approximate FWHM (i.e., 25 km) of the detector footprint. Also shown are the boundaries
878 (faint dotted lines) of the 5˚ Lunar Prospector gamma-ray dataset pixels for the region coinciding
879 with the C1XS ground track.
880

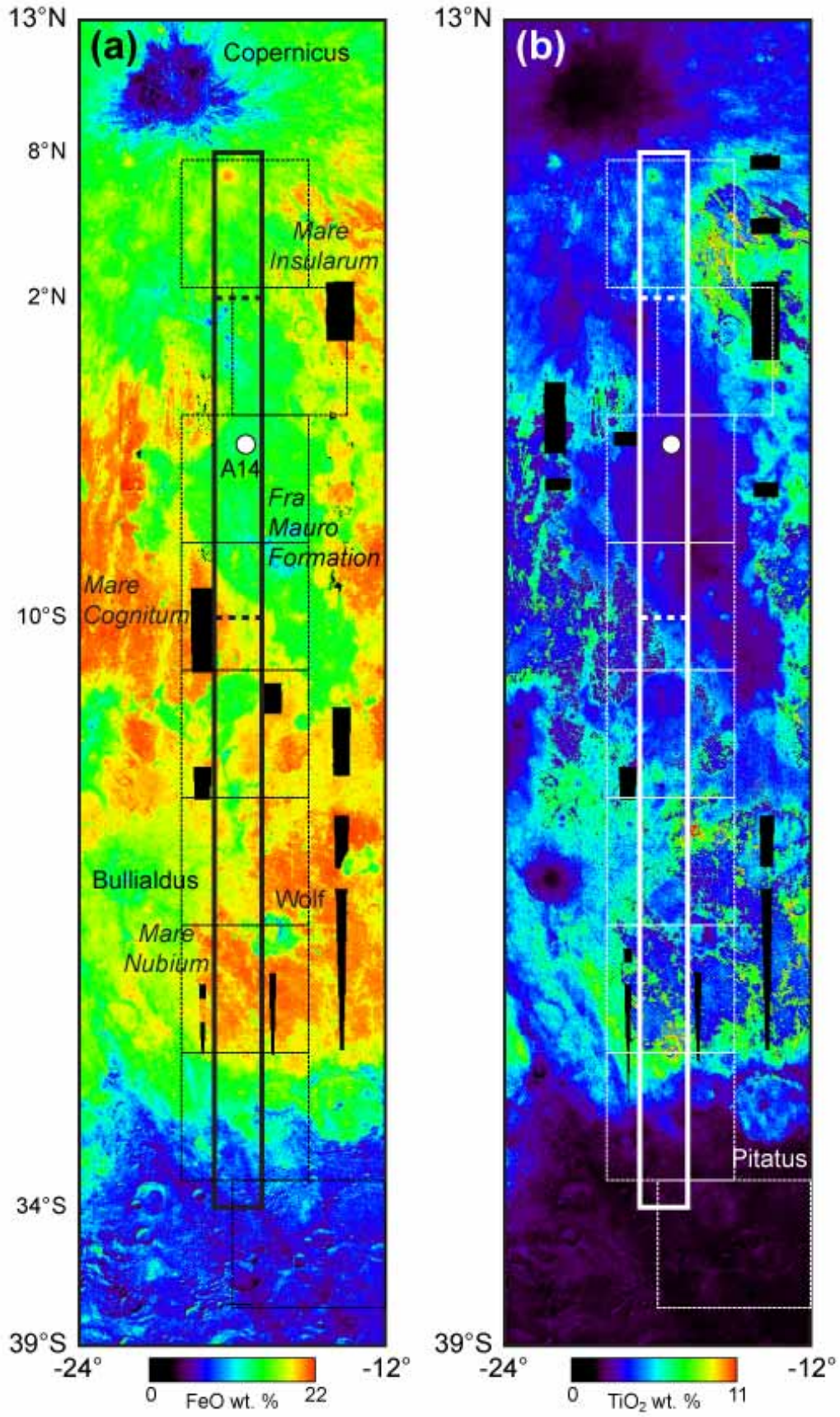
13°N
8°N
2°N
10°S
34°S
39°S
-24°
-12°
(a)
Copernicus
Mare
Insularum
A14
Fra
Mauro
Formation
Mare
Cognitum
Bullialdus
Wolf
Mare
Nubium
0
FeO wt. %
22
(b)
Pitatus
0
TiO2 wt. %
11

881

882 Figure 3. Maps of: (a) FeO wt. % and (b) TiO_2 wt. % content for the 10th January 2009 flare
883 region, derived from Clementine multispectral reflectance data according to the algorithms of
884 Gillis et al. (2004) and Gillis et al. (2003) respectively. The flare ground track (bold) and the Fra
885 Mauro Formation subsection (bold dashed lines) are indicated; the width of the outlined boxes
886 corresponds to the approximate FWHM (i.e., 25 km) of the detector footprint. Also shown are
887 the boundaries (faint dotted lines) of the 5˚ Lunar Prospector gamma-ray dataset pixels for the
888 region coinciding with the C1XS ground track.
889

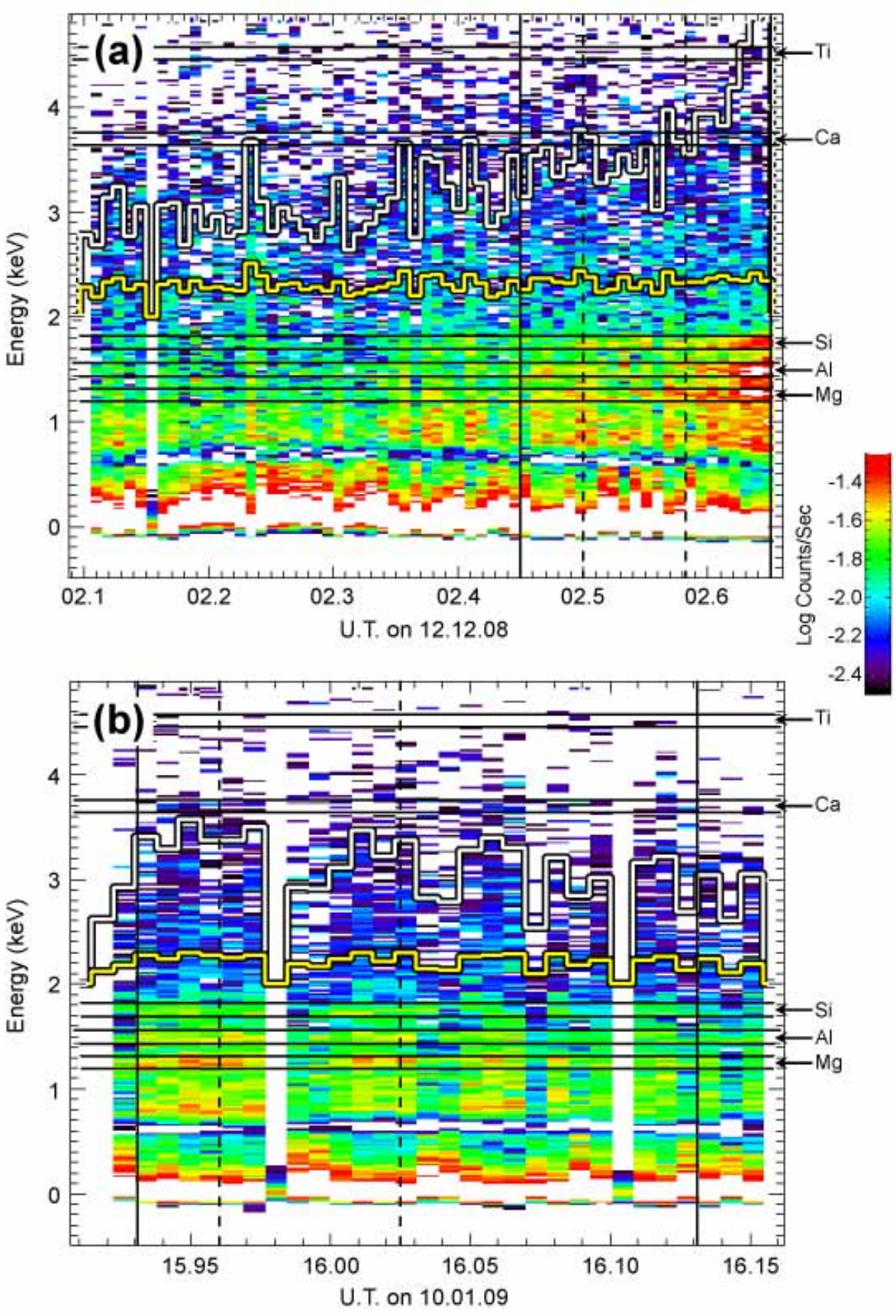
(a)
Ti
Ca
Si
Al
Mg
Energy (keV)
0
1
2
3
4
02.1
02.2
02.3
02.4
02.5
02.6
U.T. on 12.12.08
Log Counts/Sec
-1.4
-1.6
-1.8
-2.0
-2.2
-2.4
(b)
Ti
Ca
Si
Al
Mg
Energy (keV)
0
1
2
3
4
15.95
16.00
16.05
16.10
16.15
U.T. on 10.01.09

890

Figure 4. Spectrograms for the (a) 12th December 2008 and (b) 10th January 2009 flares, showing how the X-ray flux intensity varies with time and energy. The solid vertical lines indicate the start and end of each analysis; the dotted lines indicate the mare region in (a) and the Fra Mauro region in (b). The energies of the Mg, Al, Si, Ca and Ti K_α lines are indicated (note that no flux is detected for the latter two lines). The yellow and white histograms show the integrated counts in the energy ranges 1 – 2 keV and 4 – 17 keV respectively.

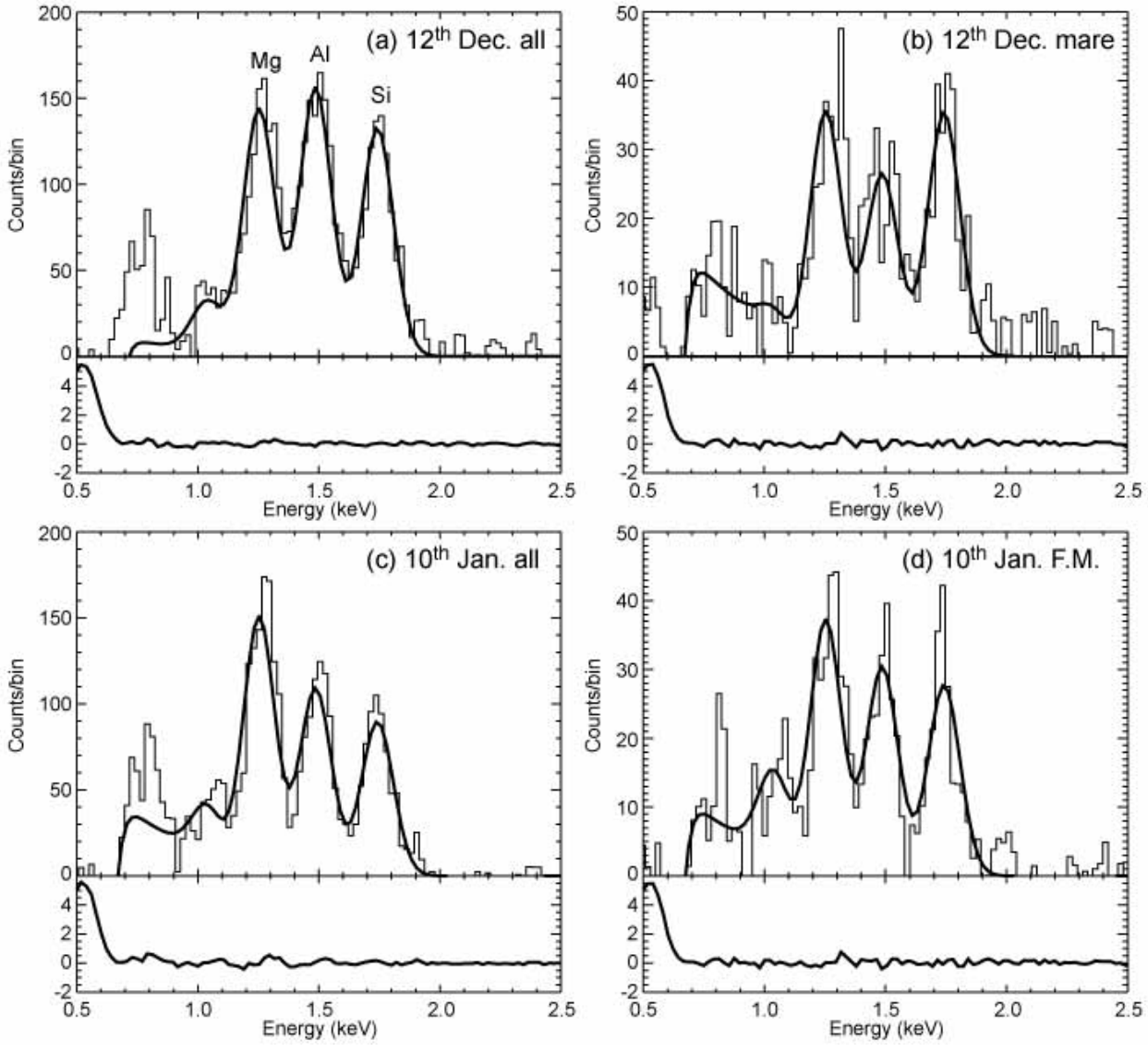

Figure 5. The background-subtracted C1XS spectra for: (a) the whole of the 12th December 2008 flare through Mare Serenitatis, (b) its mare subsection, (c) the entire 10th January 2009 flare through Mare Insularm, Mare Cognitum and Mare Nubium, and (d) the Fra Mauro Formation

902 subsection. The RAL abundance algorithm fitted model (generated using a 3.1 MK solar model)
903 for each spectrum is also shown (smooth bold line), as well as the weighted residual in each case.
904 The Mg K_α (1.25 keV), Al K_α (1.49 keV) and Si K_α (1.74 keV) peaks are clearly resolved in each
905 case. The more indistinct peak at ~1 keV may be partly due to Na K_α (1.04 keV), but likely
906 contains a contribution due to scattered solar lines (see Figure 7); the apparent 'peak' below
907 1 keV is a data processing artefact caused by instrument noise.
908

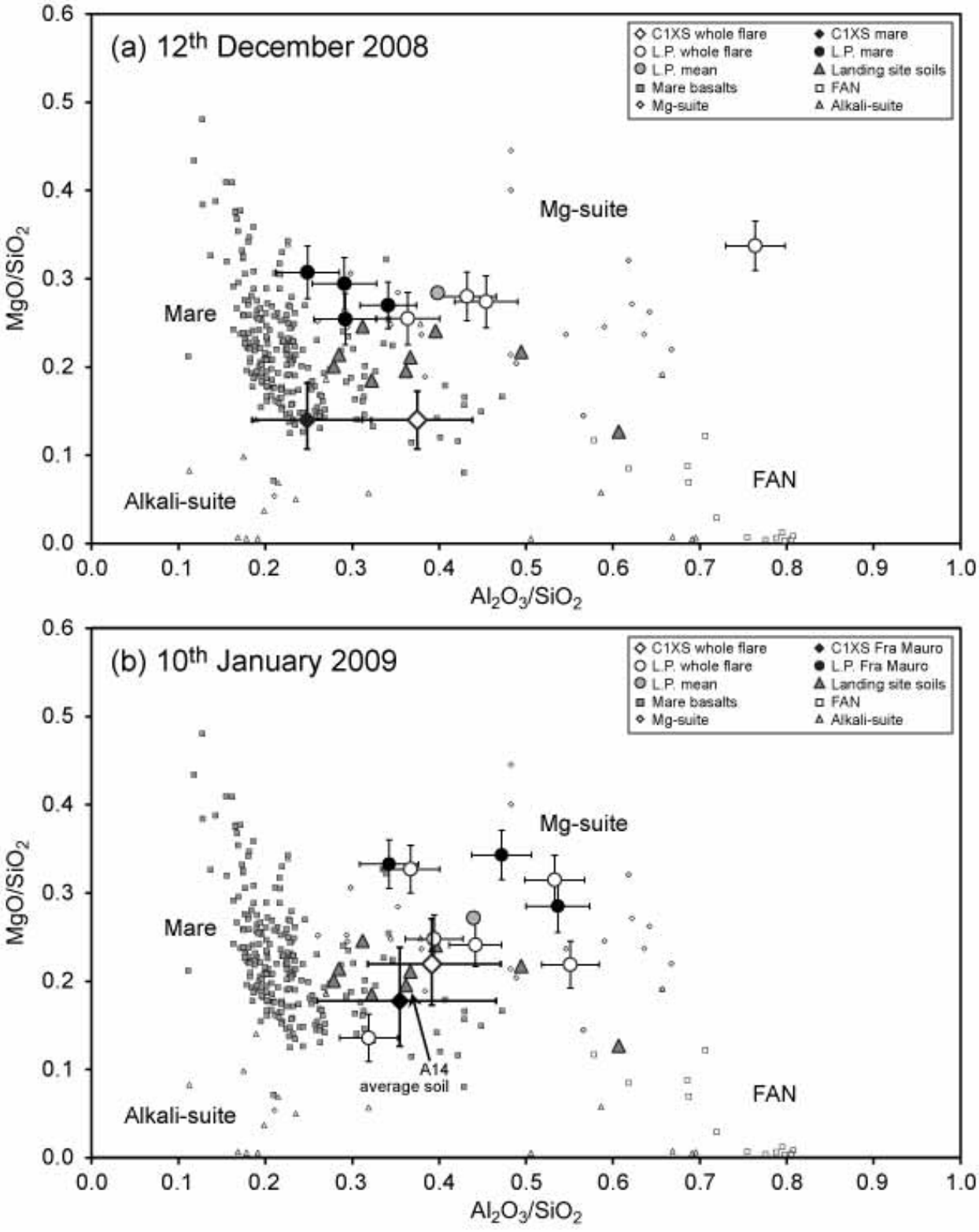

909

910 Figure 6. MgO/SiO_2 vs. Al_2O_3/SiO_2 plots showing the C1XS abundance ratios (given in Table
911 3) derived for the (a) 12th December 2008 and (b) 10th January 2009 flares. For both flares, the

912 ratio for the whole ground track is shown as well as for the subsection. The error bars on the
913 C1XS values incorporate the 1 σ fitting errors as well as the range in values provided by the two
914 flare temperature models. Also shown are: (i) the Lunar Prospector (L.P.) gamma-ray data
915 (Prettyman et al., 2006) for pixels that overlap with the flare ground tracks (as shown in
916 Figures 2 and 3); (ii) the average returned soil compositions (from Table 7.15 of McKay et al.,
917 1991) from each of the Apollo and Luna landing sites; and (iii) sample compositions of various
918 lunar lithologies: the mare basalts, ferroan anorthosites (FAN), Mg-suite and alkali suite (data
919 from Papike et al., 1998 and references therein), whose general fields are marked.
920

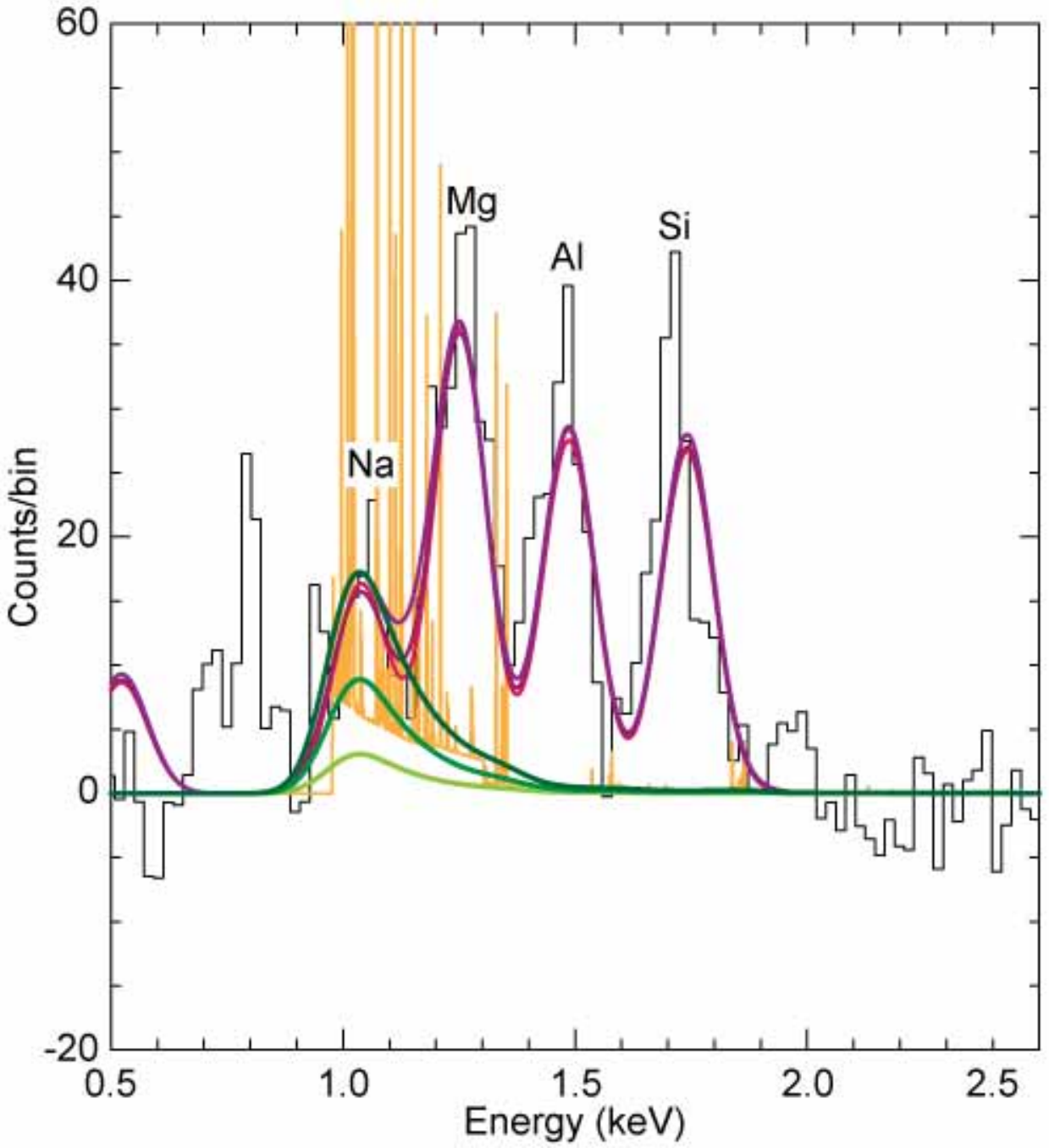

Figure 7. The possible consequences of scattered solar lines on the detection of Na K_α at 1.04 keV. The solid black line shows the data for the Fra Mauro region (as shown in Figure 5d). The orange line shows the expected energies and strengths of scattered solar lines, as predicted by the atomdb model (see Section 4); the green lines show these convolved to the C1XS resolution, allowing for a low-energy detector cut-off at 1 keV, with different levels of scattering efficiency from the lunar surface. Here we have used 0.05, 0.15 and 0.30 respectively for this

928 scattering efficiency factor. The red-purple lines are the equivalent fluorescence model
929 predictions for these background levels. Note how scattered solar lines may mimic the
930 appearance of lunar Na XRF when the scattering factor is high enough and yet the Mg, Al and Si
931 line strengths are largely unaffected. The apparent 'peak' below 1 keV in the actual data is a
932 processing artefact caused by instrument noise.
933